Environmental Science & Technology

ARTICLE

pubs.acs.org/est

Single-Particle Characterization of Summertime Antarctic Aerosols Collected at King George Island Using Quantitative Energy-Dispersive Electron Probe X-ray Microanalysis and Attenuated Total Reflection Fourier Transform-Infrared Imaging Techniques

Shila Maskey,[†] Hong Geng,[‡] Young-Chul Song,[†] HeeJin Hwang,[§] Young-Jun Yoon,[§] Kang-Ho Ahn,[∥] and Chul-Un Ro[†,*]

[†]Department of Chemistry, Inha University, Yonghyun Dong, Nam Gu, 402-751, Incheon, South Korea

[‡]Research Center of Environmental Science and Engineering, Shanxi University, Taiyuan, 030006, People's Republic of China

[§]Korea Polar Research Institute, Songdo Dong, Yeonsu Gu, 406-840, Incheon, South Korea

[∥]Department of Mechanical Engineering, Hanyang University, Sangnok Gu, 425-791, Ansan, South Korea

Supporting Information

ABSTRACT: Single-particle characterization of Antarctic aerosols was performed to investigate the impact of marine biogenic sulfur species on the chemical compositions of sea-salt aerosols in the polar atmosphere. Quantitative energy-dispersive electron probe X-ray microanalysis was used to characterize 2900 individual particles in 10 sets of aerosol samples collected between March 12 and 16, 2009 at King Sejong Station, a Korean scientific research station located at King George Island in the Antarctic. Two size modes of particles, i.e., $PM_{2.5-10}$ and $PM_{1.0-2.5}$, were analyzed, and four types of particles were identified, with sulfur-containing sea-salt particles being the most abundant, followed by genuine sea-salt particles without sulfur species, iron-containing particles, and other species including $CaCO_3$/$CaMg(CO_3)_2$, organic carbon, and aluminosilicates. When a sulfur-containing sea-salt particle showed an atomic concentration ratio of sulfur to sodium of >0.083 (seawater ratio), it is regarded as containing nonsea-salt sulfate (nss-SO_4^{2-}) and/or methanesulfonate ($CH_3SO_3^-$), which was supported by attenuated total reflection Fourier transform-infrared imaging measurements. These internal mixture particles of sea-salt/$CH_3SO_3^-$/SO_4^{2-} were very frequently encountered. As nitrate-containing particles were not encountered, and the air-masses for all of the samples originated from the Pacific Ocean (based on 5-day backward trajectories), the oxidation of dimethylsulfide (DMS) emitted from phytoplanktons in the ocean is most likely to be responsible for the formation of the mixed sea-salt/$CH_3SO_3^-$/SO_4^{2-} particles.

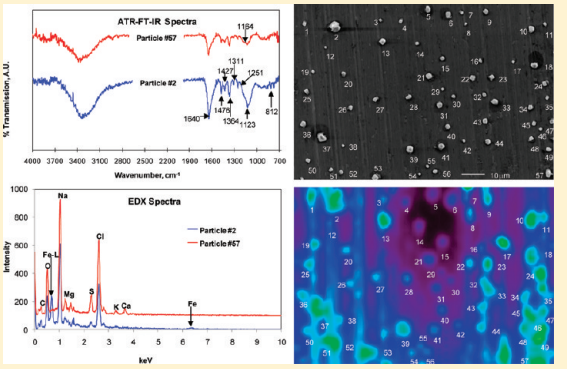

1. INTRODUCTION

The Antarctic region, isolated from anthropogenic sources, is one of the few pristine places to study natural aerosol processes and evaluate various anthropogenic impacts on the atmosphere.[1] Some studies on the characterization and seasonal cycles of different aerosol species at various Antarctic locations, such as McMurdo (Ross Island), Aboa (Queen Maud Land), Syowa (East Ongul Island), Dome Fuji (Queen Maud Land), O'Higgins (Chile), Admiralty Bay (King George Island), and Mizuho (Atka Bay) stations, have been carried out, and bulk and single-particle analytical techniques showed that sea-salts and sulfur-containing species were the most abundant constituents in Antarctic aerosol samples.[1−7] It was also reported that greater than 94% of aerosol particles in Antarctic aerosol samples were sea-salt and transformed sea-salt particles (containing excess sulfate (SO_4^{2-}) and methanesulfonate ($CH_3SO_3^-$)).[8]

However, more studies are still required to fully understand the characteristics of Antarctic aerosols. Herein, two single-particle analytical techniques, i.e., quantitative energy-dispersive electron probe X-ray microanalysis (ED-EPMA), called low-Z particle EPMA, and attenuated total reflection Fourier transform-infrared (ATR-FT-IR) imaging, were applied to characterize aerosols collected between March 12 and 16, 2009 at King Sejong Station, a Korean scientific research station located at King George Island in the Antarctic. Low-Z particle EPMA is capable of determining the chemical composition and morphology of a single atmospheric particle[9−11] and reliably analyzing

Received: March 21, 2011
Accepted: June 16, 2011
Revised: June 8, 2011
Published: June 16, 2011

ACS Publications © 2011 American Chemical Society

Table 1. Sampling Dates, Sampling Times, and Metrological Conditions at the Sampling Site

samples	sampling date	sampling time	T (°C)	RH (%)
S1	March 12, 2009	14:08−15:43	3.2−4.5	62.4−64.1
S2	March 13, 2009	13:40−14:05	3.2−3.5	65.3−65.7
S3	March 14, 2009	17:27−17:40	2.9−3.1	68.9−70.1
S4	March 15, 2009	15:44−16:01	2.5−3.2	68.8−69.3
S5	March 16, 2009	09:12−09:27	1.8−2.2	68.5−68.6

environmentally important atmospheric particles such as sulfates, nitrates, ammonium, and carbonaceous particles.[12,13] However, the low-Z particle EPMA technique has a limitation in the identification of molecular species and compounds containing hydrogen; thus sulfur-containing sea-salt particles were further investigated using ATR-FT-IR imaging as this technique can provide information on molecular species and the functional groups of individual particles.[14] The main objective of this work is to characterize summertime Antarctic aerosol particles by the use of the two single-particle analytical techniques in order to better understand aerosol properties and natural processes in a pristine environment distant from anthropogenic sources.

2. MATERIALS AND METHODS

2.1. Sampling. Aerosol samples were collected at a Korean scientific research station in the Antarctic: the King Sejong station (62°13′S, 58°47′W), which is located at King George Island, Chile (see Figure S1 of the Supporting Information). King George Island in the South Ocean is 120 km off the coast of the Antarctica, and is dominated by pervasive ice caps, with more than 90% of the island being glaciated. All samples were collected during daytime at temperatures T = 1.8−4.5 °C and relative humidity RH = 62−70% (Table 1).

Ten sets of aerosol samples were collected on Al foils (Sigma-Aldrich, 99.8% purity) during March 12 - 16, 2009 using a three stage cascade impactor (PM_{10} Impactor, Dekati Inc.). The impactor has aerodynamic cut-sizes of 10, 2.5, and 1 μm for stages 1, 2, and 3, respectively, at a 10 L min^{-1} sampling flow. To avoid collecting agglomerated particles, sampling duration was adjusted: a shorter sampling time for smaller particles and a longer time for larger ones. Overall, 2900 individual particles collected on stages 2 and 3 ($PM_{2.5-10}$ and $PM_{1.0-2.5}$ fractions with the size range of 2.5−10 μm and 1−2.5 μm, respectively) were examined.

Five-day (120 h) backward air-mass trajectories were obtained using the Hybrid Lagrangian Single-Particle Integrated Trajectory (HYSPLIT) model from the NOAA Air Resources Laboratory's web server (http://www.arl.noaa.gov/ready/hysplit4.html). The back-trajectories show that air-masses at heights of 500 m, 1000 m, and 1500 m above sea level originated from and traveled over the Pacific Ocean between March 12 and 16, 2009 (see Figure S2 of the Supporting Information).

2.2. EPMA Measurement and Data Analysis. Low-Z particle EPMA measurements were carried out on a JEOL JSM-6390 SEM equipped with an Oxford Link SATW ultrathin window energy-dispersive X-ray (EDX) detector. The resolution of the detector was 133 eV for Mn Kα X-rays. X-ray spectra were recorded under the control of INCA software (Oxford). An accelerating voltage of 10 kV, beam current of 0.5 nA, and a typical measuring time of 15 s were employed to ensure a low background level for the spectra, good sensitivity for low-Z element analysis, and statistically significant characteristic X-ray counts.[10] Morphological parameters, such as the diameter and shape factor, were calculated by an image processing routine using the INCA software. The net X-ray intensities for chemical elements were obtained by nonlinear, least-squares fitting of the collected spectra using the AXIL program.[15] The elemental concentrations of individual particles were determined from their X-ray intensities using a Monte Carlo calculation combined with reverse successive approximations.[16] By the use of the "expert system" program,[17] individual particles were classified into different groups based on their chemical compositions and morphologies. The basic classification rules are given elsewhere.[11,18]

2.3. ATR-FT-IR Imaging Technique. ATR-FT-IR imaging measurements were performed using a Perkin-Elmer Spectrum 100 FT-IR spectrometer interfaced to a Spectrum Spotlight 400 FT-IR microscope. For ATR imaging, an ATR accessory employing a germanium hemispherical internal reflection element (IRE) crystal with a diameter of 600 μm was used. A 16 × 1 pixel Mercury Cadmium Telluride (MCT) array detector was used to obtain FT-IR images with a pixel size of 1.56 μm. An ATR-FT-IR spectrum (720 to 4000 cm^{-1}) with a spectral resolution of 8 cm^{-1} was obtained for each pixel; each spectrum is an average of four coadded spectra. The position of the sample was determined using a visible light optical microscope equipped with a light-emitting diode and charge-coupled device camera. Additionally, the optical image was used to identify the same individual particles that were analyzed using low-Z particle EPMA before conducting the ATR-FT-IR imaging measurements, as optical microscopy provides an image of sufficient spatial resolution to help locate the same image field observed by low-Z particle EPMA. ATR-FT-IR imaging measurements were made for dehydrated particles as they had been under vacuum for low-Z particle EPMA measurements prior to ATR-FT-IR imaging measurements. The Ge IRE crystal was cleaned by isopropanol to avoid the contamination of the crystal surface before the ATR-FT-IR imaging measurement. A detailed description of the ATR-FT-IR imaging technique can be found in our previous paper.[14]

3. RESULTS AND DISCUSSION

3.1. Particle Types. Typical secondary electron images (SEIs) of individual particles on $PM_{2.5-10}$ and $PM_{1.0-2.5}$ samples are shown in Figure 1, where the chemical species making up each particle is indicated. The relative abundances of all particle types, which were classified based on their X-ray spectra and SEI data of individual particles, are shown in Table 2. The characteristics of various particle types are described as follows.

3.2. Genuine Sea-Salt Particles without Sulfur Species. Sea-salt aerosols are produced at the ocean surface, are ubiquitous in the marine boundary layer (MBL), can act as a source of reactive halogen species and cloud condensation nuclei (CCN), and can cause atmospheric scattering of solar radiation.[19] Genuine sea-salt particles that did not experience atmospheric chemical reactions after being emitted into the air have SEI that are bright and cubic in shape (e.g., particles #1, #5, #6, #17, and #25 in Figure 1). Their X-ray spectra are dominated by Na and Cl X-ray peaks (Figure S3a of the Supporting Information, SI), often together with small peaks from C, O, and/or Mg. The atomic Mg/Na concentration ratios are 0.086 and 0.114 on weighted average for $PM_{2.5-10}$ and $PM_{1.0-2.5}$ aerosols, respectively (Tables S1 and S2 of the SI), which are close to 0.119, i.e., the seawater [Mg]/[Na] ratio; but the atomic Cl/Na

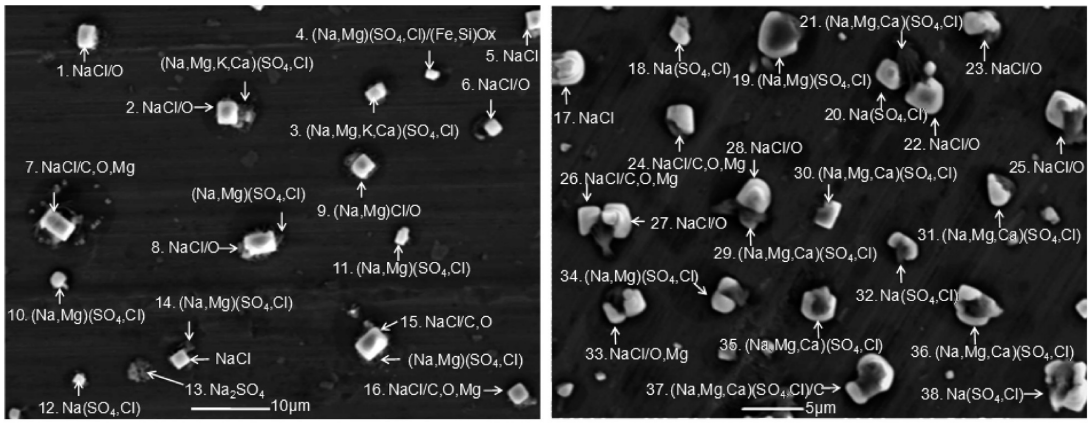

(a) Particles #1-#16, deposited on stage 2 (from sample S1) (b) Particles #17-#38, deposited on stage 3 (from sample S1)

Figure 1. Typical secondary electron images of aerosol particles collected at King Sejong station, Antarctica. (a) Particles #1−#16, deposited on stage 2 (from sample S1) ; (b) Particles #17−#38, deposited on stage 3 (from sample S1).

Table 2. Particle Types and Their Relative Abundances in $PM_{2.5-10}$ and $PM_{1.0-2.5}$ Fractions, Respectively, for the Samples S1−S5

particle types	relative abundances in $PM_{2.5-10}$ fraction (%)						relative abundances in $PM_{1.0-2.5}$ fraction (%)					
	S1	S2	S3	S4	S5	ave	S1	S2	S3	S4	S5	ave
1. genuine sea-salts without sulfur	**47.9**	**42.1**	**43.0**	**23.2**	**48.4**	**40.9**	**17.3**	**38.0**	**38.6**	**10.2**	**20.8**	**25.0**
NaCl	3.5	7.2	0.0	0.7	0.6	2.4	0.6	6.3	0.8	0.6	0	1.7
NaCl/O	22.6	28.9	12.1	18.9	26.8	21.9	12.6	22.9	26.1	4.5	5.8	14.4
NaCl/O,Mg	4.2	1.4	2.0	1.3	1.9	2.2	0.7	2.5	2.5	0.0	0.8	1.3
NaCl/C,O	6.3	0.0	9.4	0.9	1.3	3.6	2.7	1.9	6.7	2.6	4.2	3.6
NaCl/C,O,Mg	11.3	4.6	19.5	1.4	17.8	10.9	0.7	4.4	2.5	2.5	10.0	4.0
2. sulfur-containing sea-salts	**48.6**	**55.3**	**55.0**	**75.4**	**47.1**	**56.3**	**78.1**	**59.5**	**55.5**	**87.2**	**72.5**	**70.6**
(1) [S]/[Na]≤0.083	27.5	34.8	22.8	41.2	25.5	30.4	59.7	39.9	49.6	64.8	50.9	53.0
$Na(SO_4,Cl)$	1.4	3.9	1.3	3.6	3.2	2.7	2.7	1.3	16.8	7.1	1.7	5.9
$(Na,Mg)(SO_4,Cl)$	9.2	12.5	1.3	8.7	8.3	8.0	14.6	7.0	13.4	5.8	4.2	9.0
$Na(SO_4,Cl)/C$	0.0	0.0	0.7	1.4	0.0	0.4	2.0	0.0	3.4	6.4	4.2	3.2
$(Na,Mg)(SO_4,Cl)/C$	16.9	18.4	19.5	27.5	14.0	19.3	40.4	31.6	16.0	45.5	40.8	34.9
(2) [S]/[Na]>0.083	21.1	20.5	32.2	34	21.7	25.9	18.5	19.7	5.8	22.9	21.7	17.7
$(Na,Mg,Ca)(SO_4,Cl)$	1.4	6.6	1.3	7.2	1.9	3.7	1.3	1.3	0.8	0.6	0.0	0.8
$(Na,Mg,K,Ca)(SO_4,Cl)$	3.5	2.0	0.0	2.9	1.3	1.9	0.0	0.0	0.0	0.6	4.2	1.0
$(Na,Mg,K,Ca)(SO_4,Cl)/C$	7.0	2.0	2.0	2.9	5.8	3.9	1.3	2.5	1.6	5.7	5.8	3.4
$(Na,Mg,Ca)(SO_4,Cl)/C$	9.2	9.9	28.9	21.0	12.7	16.3	15.9	15.9	3.4	16.0	11.7	12.6
3. Fe-containing particles	**2.1**	**2.6**	**1.3**	**1.4**	**1.3**	**1.7**	**3.3**	**1.9**	**5.9**	**2.6**	**5.0**	**3.7**
4. others	**1.4**	**0.0**	**0.7**	**0.0**	**3.2**	**1.1**	**1.3**	**0.6**	**0.0**	**0.0**	**1.7**	**0.7**
sum	**100**	**100**	**100**	**100**	**100**	**100**	**100**	**100**	**100**	**100**	**100**	**100**

concentration ratios, which are 0.861 and 0.787 on weighted average for $PM_{2.5-10}$ and $PM_{1.0-2.5}$ aerosols, respectively (Tables S1 and S2 of the SI), are somewhat lower than the seawater [Cl]/[Na] ratio (1.16). Organic species present in the sea-salt particles, inferred from carbon (∼4−12 at%, on average) and oxygen signals in their X-ray spectra, possibly result from biogenic species and/or humic or humic-like substances in the marine environment. Some of the oxygen species might come from water inside the particles and the NaOH shell, an alkaline hygroscopic coating around NaCl.[20] Herein, the genuine sea-salt particles without sulfur were further classified into five types, based on their X-ray signals from C, O, and other minor elements (Table 2 and Tables S1 and S2 of the SI). They include NaCl, NaCl/O, NaCl/(Mg,O), NaCl/(C,O), and NaCl/(C,O,Mg) and look similar on their SEIs (e.g., particles #1, #5, #16, and #33 in Figure 1, respectively).

3.3. Sulfur-Containing Sea-Salt Particles. Many sea-salt particles have a sulfur peak in their X-ray spectra (Table 2 and Figures S3b and S3c of the SI). These sulfur-containing sea-salt particles include two categories. One is for particles whose atomic S/Na concentration is ≤0.083, i.e., the seawater [S]/[Na] ratio.[21] They contain $Na(SO_4, Cl)$, $Na(SO_4, Cl)/C$, $(Na, Mg)(SO_4, Cl)$, and $(Na, Mg)(SO_4, Cl)/C$, where the [S]/[Na] ratio is on average ∼0.048 (Tables S1 and S2 of the SI) and the [O]/[Na] ratio is ∼0.3−1.1 (0.526 and 0.506 on weighted average in $PM_{2.5-10}$ and $PM_{1.0-2.5}$ fractions, respectively). Thus, their sulfur signals are regarded to be from sea-salt sulfate ($ss\text{-}SO_4^{2-}$). Another category is for particles whose atomic [S]/[Na] ratio is >0.083, such as $(Na, Mg, Ca)(SO_4, Cl)$, (Na, Mg,

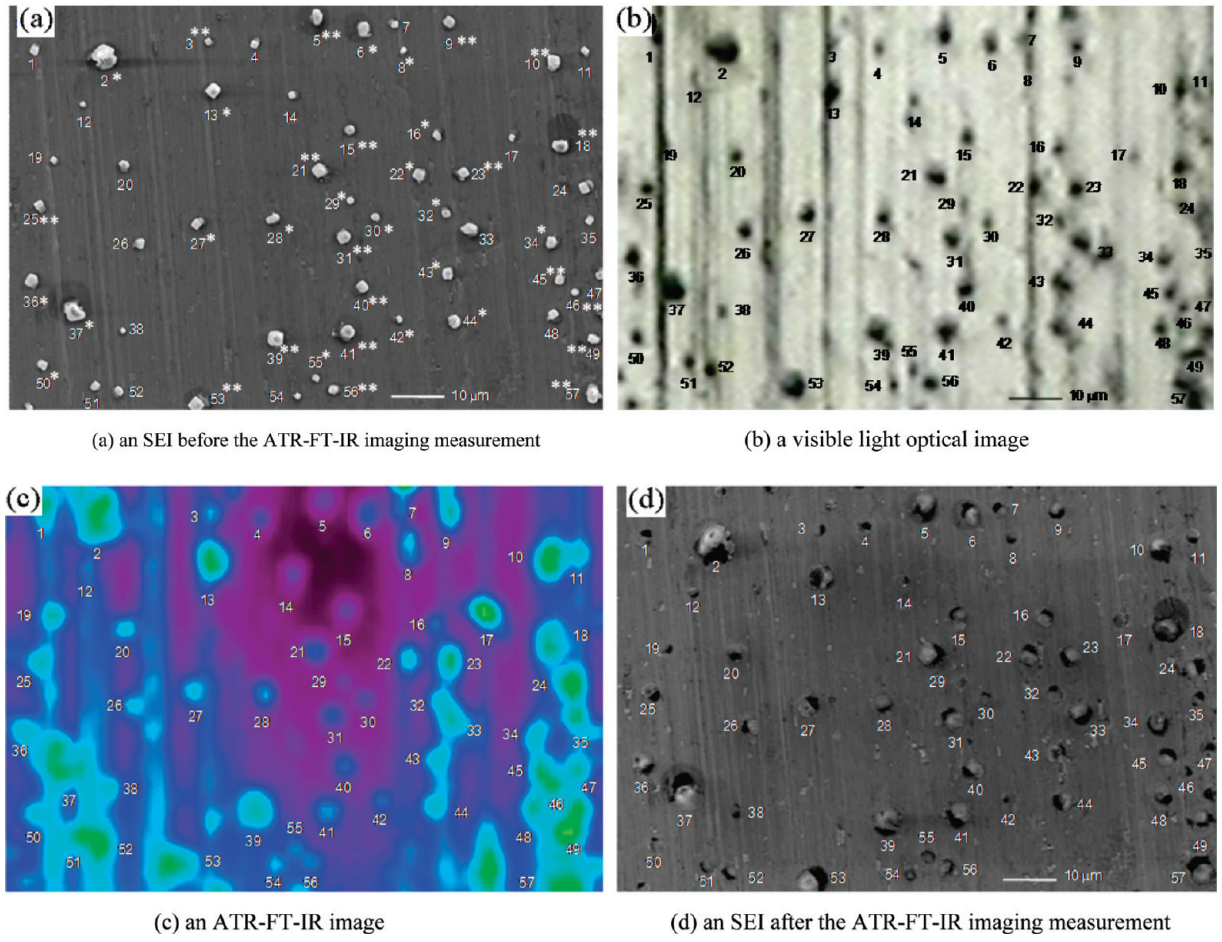

(a) an SEI before the ATR-FT-IR imaging measurement

(b) a visible light optical image

(c) an ATR-FT-IR image

(d) an SEI after the ATR-FT-IR imaging measurement

Figure 2. Comparison of the secondary electron images (SEIs) and ATR-FT-IR image of the same 57 individual airborne particles on stage 2 for the sample S2 (the particles without additional label are genuine sea-salt particles, the particles labeled with * are sulfur-containing sea-salt particles with [S]/[Na] ≤ 0.083, and the particles labeled with ** are sulfur-containing sea-salt particles with [S]/[Na] > 0.083).

Ca, K)(SO_4, Cl), (Na, Mg, Ca)(SO_4, Cl)/C, and (Na, Mg, K, Ca)(SO_4, Cl)/C. The average [S]/[Na] ratio is ∼0.1−0.3 (0.167 and 0.210 on weighted average in $PM_{2.5-10}$ and $PM_{1.0-2.5}$, respectively, see Tables S1 and S2 of the SI), indicating that the additional sulfur comes from other sources, such as nss-SO_4^{2-} (e.g., Na_2SO_4 and (Na, Mg)SO_4) and/or $CH_3SO_3^-$. They are likely to be the reaction products of genuine sea-salt with SO_2/H_2SO_4 and/or methylsulfonic acid (MSA) from the oxidation of dimethylsulfide (DMS).[22] The [O]/[Na] ratio is ∼0.5−4.2 (1.146 and 1.297 on weighted average in $PM_{2.5-10}$ and $PM_{1.0-2.5}$, respectively). The [S]/[Na] ratio increases with a decrease in particle size: (0.167 vs 0.210). This suggests that the reactions occurred more frequently for smaller particles due to their larger area/volume ratio.

The core−shell sea-salt particles (e.g., particles #2, #8, #14, #15, #19, #31, #35, and #36 in Figure 1) indicates that they might be in the form of liquid droplets at the time of collection.[23] When water evaporated from the collected sea-salt particles, crystalline NaCl particles were fractionally or wholly crystallized out. The liquid content would provide an enhanced capacity for soluble species in the reactions.[22] Kukui et al. reported that MSA, the major oxidized end product of DMS, would be produced by liquid-phase reactions and that the water-soluble intermediate products from the oxidation of DMS would contribute to the growth of existing particles.[24] This is consistent with our observation, in that the X-ray spectra data obtained from the shell (darkly shaded) particles showed the sulfur species.

To further determine sulfur species existing in the sulfur-containing sea-salt particles, some particles on stage 2 for sample S2 were investigated by ATR-FT-IR imaging, since the relative abundances of particles with [S]/[Na] ≤ 0.083 and particles with [S]/[Na] > 0.083 in the $PM_{2.5-10}$ fraction of sample S2 are close to their respective overall average abundance (Table 2). Figure 2 shows an SEI obtained prior to ATR-FT-IR imaging measurement (Figure 2(a)), a visible light optical image (Figure 2(b)), an ATR-FT-IR image (Figure 2(c)), and an SEI after ATR-FT-IR imaging measurement (Figure 2(d)) for the same 57 airborne particles. First, the morphologies and chemical compositions of all the particles on the image field were obtained by low-Z particle EPMA. Then, the ATR-FT-IR image was obtained by the application of principle component analysis (PCA) after the first differentiation of the original ATR-FT-IR spectra across all of the pixels in the image. Although the quality of the SEI and ATR-FT-IR images differ due to the inherently different spatial resolutions of the images (∼100 nm for SEIs and 3.1 μm for the ATR-FT-IR images), the same particle patterns ensured that the same particles were probed. The area of each image is ∼120 × 80 μm^2. Considering that the pixel size of the ATR-FT-IR image is 1.56 × 1.56 μm^2, the number of pixels for the ATR-FT-IR image shown is ∼3940. An IR spectrum (4000−720 cm^{-1}) is recorded

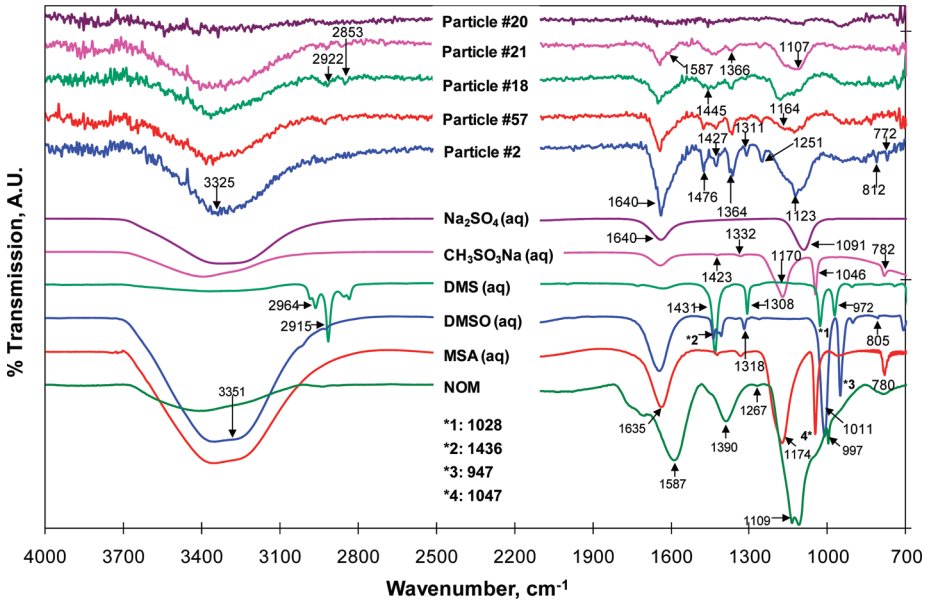

Figure 3. ATR-FT-IR spectra of aerosol particles and standard materials (Na_2SO_4, CH_3SO_3Na, DMS, DMSO, MSA, and natural organic matter (NOM)). Data from the 2200−2390 cm^{-1} region, where atmospheric CO_2 peaks are present, were deleted for clarity.

for each pixel in the image. The manufacturer's software interpolates ATR-FT-IR imaging pixel data onto a display image with many more pixels, such that the final display image looks better than the actual image.

The SEIs (Figure 2(a),(d)) clearly show the morphologies and locations of the 57 particles before and after the ATR-FT-IR imaging measurements. For the ATR-FT-IR imaging measurement, the sample has to be in contact with the IRE crystal so that some force is applied to the sample during contact. When good contact is made and the sample is well pressed against the IRE crystal, the particles were (partly or fully) embedded into the ductile Al collecting foil.

The ATR-FT-IR spectra for all of the pixels in the image were considered in the PCA analysis. Similar spectra with significant encountering frequencies were grouped as a principle component. Low-*Z* particle EPMA and ATR-FT-IR image data indicate that two types of particles (two principle components) are dominant: 19 genuine sea-salt particles and 38 sulfur-containing sea-salt particles (see Figure 2 and Table S4 of the SI). Since NaCl species is IR inactive, 19 genuine sea-salt particles do not show any significant IR peak (see ATR-FT-IR spectrum of an exemplar genuine sea-salt particle #20 in Figure 3). Typical ATR-FT-IR spectra of the sulfur-containing particles are also shown in Figure 3, in which particle #2 is the one with [S]/[Na] < 0.083 while particles #18, #21, and #57 are those with [S]/[Na] > 0.083 (see Table S4 of the SI). The spectra for the four particles are similar at a glance. Each spectrum shows IR absorption peaks at 3325, 1640, 1364, 1251, and 1123 cm^{-1}. However, the spectra of particle #2 are somewhat different from those of particles #18, #21 and #57: IR peaks at 1476, 1427, 1311, 1251, 1123, and 1640 cm^{-1} are stronger in the spectra of particle #2, whereas IR peaks at 2922 and 2853 cm^{-1} are stronger in those of particles #18, #21, and #57. ATR-FT-IR spectra of all 38 sulfur-containing particles belong to one of the two types. Overall, the peak height (in A) of SO_4^{2-} IR peak at ~1123 cm^{-1} on average in genuine sea-salt particles (0.012 ± 0.002) is lower than that in sulfur-containing sea-salt particles (0.031 ± 0.012) (Table S4 of the SI).

ATR-FT-IR spectra measured for aqueous solutions of Na_2SO_4, CH_3SO_3Na, DMS, dimethyl sulfoxide (DMSO), and MSA (purchased from Aldrich) are also shown in Figure 3. These chemicals are reported to be intermediate or final chemicals in the formation of nonsea-salt sulfates from phytoplankton activities.[25,26] In addition, an ATR-FT-IR spectrum obtained from Natural Organic Matter (NOM) powders (purchased from International Humic Substance Society) is shown in Figure 3. The NOM sample is reported to have been obtained from a drinking water reservoir at Skarnes, Norway and contain humic and fulvic substances. The broad IR peaks seen at ~3325 and ~1640 cm^{-1} in the ATR-FT-IR spectra of all particles (except DMS) are from the O−H vibrations of water molecule. Although the SEIs of the particles show that they look crystalline, it is clear that a significant amount of water exists in the particles according to ATR-FT-IR analysis. The IR peaks at 2922 and 2853 cm^{-1} are from DMS molecule, which is contained in particles #18, #21, and #57. The peak at 1640 cm^{-1} is too broad to be only from water molecule; it seems that another IR peak at 1587 cm^{-1} (NOM) is convoluted with the peak at 1640 cm^{-1}. IR peaks at 1476, 1364, 1251, and 812 cm^{-1} seem to be from biogenic species and/or humic or humic-like substances in the marine environment. The peaks at 1427 and 1311 cm^{-1} are either from DMS or DMSO molecules. A very broad, strong peak in the 1190−1040 cm^{-1} region seems to have merged with the two IR peaks arising from SO_3^{2-} of CH_3SO_3Na at ~1046 and ~1170 cm^{-1}, and also with that at ~1091 cm^{-1} from SO_4^{2-} of Na_2SO_4. Hopkins et al. reported that substantial heterogeneous replacement of chloride by $CH_3SO_3^-$ and nss-SO_4^{2-} in sea-salt particles (with characteristic ratios of nss-S/Na > 0.10 and $CH_3SO_3^-$/nss-SO_4^{2-} > 0.6) occurred at low temperatures (T < 15 °C).[22] The IR peaks of MSA at 1174 and 1047 may also have merged into the broad IR peak in the 1190−1040 cm^{-1} region. The sharp IR peak at 1123 cm^{-1} in the ATR-FT-IR spectra of particle #2 indicates that it likely only contains ss-SO_4^{2-}. It suggests that the sulfur-containing sea-salt particles with [S]/[Na] ≤0.083 can be distinguished from those with [S]/[Na] > 0.083 by their ATR-FT-IR spectra. The peaks at 1587, 1390, and 1109 cm^{-1} in the NOM ATR-FT-IR

spectrum indicate that biogenic species and/or humic or humic-like substances are likely mixed with the sulfur-containing sea-salt particles. It is consistent with the EPMA measurement results (the carbonaceous species was often detected in genuine and sulfur-containing sea-salt particles as shown in Tables S1 and S2 of the SI). The sulfur species in the sulfur-containing particles seem to be complex mixtures of SO_4^{2-}, $CH_3SO_3^-$, DMS, DMSO, MSA, and NOM-like species.

3.4. Fe-Containing Particles. Fe-containing particles have irregular shapes in their SEIs, including FeO_x particles and Fe/FeO_x particles internally mixed with sea-salts (particle #4 in Figure 1). The atomic concentrations of Fe are in the range 1−80 at%, as shown in Table S3 and Figure S4 of the SI. The observation that many of them (especially for particles in $PM_{1.0-2.5}$ fraction) are coupled with S suggests that the Fe-containing particles are likely to have come from the seawater. Much research has shown that in seawater, especially when phytoplankton blooms occur, there is a close link between Fe and S.[27,28] In "High-Nutrient, Low-Chlorophyll"(HNLC) areas such as the Southern Ocean where external Fe inputs are low, sea ice might be a significant pool of bioavailable Fe in the Antarctic surface waters.[29] In addition, as soil particles (e.g., aluminosilicates) are rarely encountered in these samples, Fe-containing particles are not likely to be of soil origin.

3.5. Other Species. We classified the particles which did not belong to the above types into the "other species" group because they were observed in all samples very infrequently (<1%). They include $CaCO_3$/$CaMg(CO_3)_2$, carbonaceous (mostly organic compounds), and aluminosilicate-containing particles. It seems that most of them originated from the ocean (i.e., biogenic particles) and a very few originated from the local land (i.e., $CaCO_3$/$CaMg(CO_3)_2$ and aluminosilicate-containing particles).

3.6. Relative Abundances of Various Particle Types. The relative abundances of major particle types are shown in Table 2. Sea-salt particles, including both genuine and sulfur-containing species, are the most frequently encountered, with relative abundances of 97.1% and 95.6% on average in the $PM_{2.5-10}$ and $PM_{1.0-2.5}$ fractions, respectively. The sulfur-containing sea-salt particles outnumber the genuine ones: relative abundances of 56.3% vs. 40.9% on average in the $PM_{2.5-10}$ fraction and 70.6% vs. 25.0% in the $PM_{1.0-2.5}$ fraction. For the sulfur-containing sea-salt particles, those with $[S]/[Na] \leq 0.083$ are more abundant than those with $[S]/[Na] > 0.083$: 30.4% vs. 25.9% on average in the $PM_{2.5-10}$ fraction and 53.0% vs. 17.7% in the $PM_{1.0-2.5}$ fraction, respectively. This suggests that a significant fraction of the sulfur in many sulfur-containing sea-salt particles also came from ss-SO_4^{2-}. The five-day air-mass back-trajectories at heights of 500, 1000, and 1500 m (Figure S2 of the SI) indicate that the air-masses for all of the samples originated from the Pacific Ocean and arrived at the sampling site with westerly wind, implying seawater from the Pacific Ocean should be the only source of the aerosol particles. The relative abundances of genuine sea-salt particles without sulfur on average in the $PM_{1.0-2.5}$ fractions of samples S1−S5 are smaller than those in the $PM_{2.5-10}$ fractions, revealing that smaller sea-salt particles tend to contain sulfur/sulfate than larger ones. The variations of relative abundances among different samples (S1−S5) (especially in the $PM_{1.0-2.5}$ fractions), as shown in Table 2, might be attributed to different local temperatures, RHs, atmospheric pressures, waves, etc.

Fe-containing particles show relative abundances of 1.7% on average in the $PM_{2.5-10}$ fraction (2.6% maximum in sample S2) and 3.7% on average in the $PM_{1.0-2.5}$ fraction (5.9% maximum in sample S3).

3.7. Possible Mechanisms for the Formation of SO_4^{2-}/$CH_3SO_3^-$-containing Sea-Salt Particles in the Antarctic Region. In the austral summer (November−March) of the Antarctic, higher solar radiation levels and temperatures tend to enhance phytoplankton activities and, thus, enhance the production and emission of oceanic DMS.[30−32] The volatile DMS diffuses into the atmosphere and undergoes complex sequences of gas-phase oxidation reactions, generating various sulfur-containing products such as DMSO, MSA, SO_2, and H_2SO_4.[25,26] These oxidized products can condense onto preexisting particles (primarily sea salt particles), resulting in changes in the particle compositions and sizes.[24] From the Antarctic aerosol particles' chemical compositions and relative abundances, we deduced that the nss-SO_4^{2-}/$CH_3SO_3^-$-containing sea-salt particles were generated by reactions of the sea-salt particles with MSA and/or H_2SO_4 from biogenic sources rather than anthropogenic ones. The reasons are as follows:

(1) Among all of the analyzed individual particles, no nitrate-containing sea-salt particle was encountered, i.e., none of the X-ray spectra showed a nitrogen (N) peak. It has been rarely reported that in the urban atmosphere, where anthropogenic sources are abundant, air pollutants contain only sulfur species without nitrogen species. The mass concentration of airborne NO_x is usually larger than that of SO_2 in the urban atmosphere, and ambient NO_x has a higher reactivity than SO_2.[13] Our previous study reported that the summertime Arctic aerosols contained more nitrate than sulfate, indicating the anthropogenic influence on the Arctic aerosols.[12]

(2) The air-mass back-trajectories at heights of 500, 1000, and 1500 m showed that the air-masses for all the samples originated from the Pacific Ocean (Figure S2 of the SI), indicating that the source of aerosol particles was of marine origin.

(3) It was reported that phytoplankton bloom could occur in the austral summer of the Southern Ocean, resulting in promoted emissions of DMS in this region.[32] As Fe supply controls phytoplankton growth and community composition during the summer in the polar Southern Ocean waters,[27] our observation of a significant amount of Fe-containing particles (Table 2) suggests that oceanic phytoplankton might bloom during the sampling days.

(4) Other obvious sources of volatile sulfurs (e.g., volcano eruptions) were absent during the sampling period in this region and the surrounding area.

Our conclusion is that the aerosols over King George Island were influenced by natural sources during the sampling period: airborne SO_2/H_2SO_4 and MSA produced from the oxidation of DMS of marine origin contributed to the formation of nss-SO_4^{2-}/$CH_3SO_3^-$-containing sea-salt particles. The low-Z particle EPMA combined with ATR-FT-IR measurements can be used to differentiate ss-SO_4^{2-}-containing sea-salt particles from nss-SO_4^{2-}/$CH_3SO_3^-$-containing ones and for the detailed characterization of the coastal aerosols in the marine boundary layer (MBL).

■ ASSOCIATED CONTENT

Supporting Information. Tables S1−S4 and Figures S1− S4 are available in the Supporting Information. This

material is available free of charge via the Internet at http://pubs.acs.org.

AUTHOR INFORMATION

Corresponding Author
*Phone: +82 32 860 7676; Fax: +82 32 867 5604; E-mail: curo@inha.ac.kr.

ACKNOWLEDGMENT

This research was supported by Basic Science Research Program through the National Research Foundation of Korea (NRF) funded by the Ministry of Education, Science and Technology (2010-0018881) and by the funds of the SAM Project (PE11010 of Korea Polar Research Institute).

REFERENCES

(1) Préndez, M.; Wachter, J.; Vega, C.; Flocchini, R. G.; Wakayabashi, P.; Morales, J. R. $PM_{2.5}$ aerosols collected in the Antarctic Peninsula with a solar powered sampler during austral summer periods. *Atmos. Environ.* **2009**, *43* (34), 5575–5578.

(2) Shaw, G. E. Antarctic aerosols: A review. *Rev. Geophys.* **1988**, *26* (1), 89–112.

(3) Hara, K.; Iwasaka, Y.; Wada, M.; Ihara, T.; Shiba, H.; Osada, K.; Yamanouchi, T. Aerosol constituents and their spatial distribution in the free troposphere of coastal Antarctic regions. *J. Geophys. Res.* **2006**, *111* (D15), D15216.

(4) Kerminen, V.-M.; Teinilä, K.; Hillamo, R. Chemistry of sea-salt particles in the summer Antarctic atmosphere. *Atmos. Environ.* **2000**, *34* (17), 2817–2825.

(5) Rathke, C.; Notholt, J.; Fischer, J.; Herber, A. Properties of coastal Antarctic aerosol from combined FTIR spectrometer and sun photometer measurements. *Geophys. Res. Lett.* **2002**, *29* (23), 2131.

(6) Hara, K.; Osada, K.; Kido, M.; Hayashi, M.; Matsunaga, K.; Iwasaka, Y.; Yamanouchi, T.; Hashida, G.; Fukatsu, T. Chemistry of sea-salt particles and inorganic halogen species in Antarctic regions: Compositional differences between coastal and inland stations. *J. Geophys. Res.* **2004**, *109* (D20), D20208.

(7) Biancato, D.; Ceccato, D.; Chiminello, F.; Mittner, P. Micro-PIXE and principal component analysis in a study of internal mixing phenomena in Antarctic coastal aerosol. *Nucl. Instrum. Methods B* **2006**, *249* (1−2), 561–565.

(8) Wouters, L.; Artaxo, P.; Van Grieken, R. Laser microprobe mass analysis of individual Antarctic aerosol particles. *Intern. J. Environ. Anal. Chem.* **1990**, *38* (3), 427–438.

(9) Ro, C.-U.; Hwang, H.; Kim, H.; Chun, Y.; Van Grieken, R. Single-particle characterization of four "Asian dust" samples collected in Korea, using low-*Z* particle electron probe X-ray microanalysis. *Environ. Sci. Technol.* **2005**, *39* (6), 1409–1419.

(10) Ro, C.-U.; Osán, J.; Van Grieken, R. Determination of low-*Z* elements in individual environmental particles using windowless EPMA. *Anal. Chem.* **1999**, *71* (8), 1521–1528.

(11) Ro, C.-U.; Osán, J.; Szalóki, I.; Oh, K.-Y.; Kim, H.; Grieken, R. V. Determination of chemical species in individual aerosol particles using ultrathin window EPMA. *Environ. Sci. Technol.* **2000**, *34* (14), 3023–3030.

(12) Geng, H.; Ryu, J.; Jung, H. J.; Chung, H.; Ahn, K. H.; Ro, C.-U. Single-particle characterization of summertime arctic aerosols collected at Ny-Alesund, Svalbard. *Environ. Sci. Technol.* **2010**, *44* (7), 2348–2353.

(13) Geng, H.; Park, Y.; Hwang, H.; Kang, S.; Ro, C. U. Elevated nitrogen-containing particles observed in Asian dust aerosol samples collected at the marine boundary layer of the Bohai Sea and the Yellow Sea. *Atmos. Chem. Phys.* **2009**, *9* (18), 6933–6947.

(14) Song, Y.-C.; Ryu, J.; Malek, M. A.; Jung, H.-J.; Ro, C.-U. Chemical speciation of individual airborne particles by the combined use of quantitative energy-dispersive electron probe X-ray microanalysis and attenuated total reflection Fourier transform-infrared imaging techniques. *Anal. Chem.* **2010**, *82* (19), 7987–7998.

(15) Vekemans, B.; Janssens, K.; Vincze, L.; Adams, F.; Van Espen, P. Analysis of X-ray spectra by iterative least squares (AXIL): New developments. *X-Ray Spectrom.* **1994**, *23* (6), 278–285.

(16) Ro, C.-U.; Osán, J.; Szalóki, I.; de Hoog, J.; Worobiec, A.; Grieken, R. V. A Monte Carlo program for quantitative electron-induced X-ray analysis of individual particles. *Anal. Chem.* **2003**, *75* (4), 851–859.

(17) Ro, C.-U.; Kim, H.; Van Grieken, R. An expert system for chemical speciation of individual particles using low-Z particle electron probe X-ray microanalysis data. *Anal. Chem.* **2004**, *76* (5), 1322–1327.

(18) Ro, C.-U.; Oh, K. Y.; Kim, H. K.; Kim, Y. P.; Lee, S. B.; Kim, K. H.; Chang, H. K.; Osan, J.; de Hong, J.; Worobiec, A.; Van Grieken, R. Single-particle analysis of aerosols at Cheju Island, Korea, using low-Z electron probe X-ray microanalysis: A direct proof of nitrate formation from sea salts. *Environ. Sci. Technol.* **2001**, *35* (22), 4487–4494.

(19) Hara, K.; Osada, K.; Kido, M.; Matsunaga, K.; Iwasaka, Y.; Hashida, G.; Yamanouchi, T. Variations of constituents of individual sea-salt particles at Syowa station, Antarctica. *Tellus B* **2005**, *57* (3), 230–246.

(20) Laskin, A.; Gaspar, D. J.; Wang, W.; Hunt, S. W.; Cowin, J. P.; Colson, S. D.; Finlayson-Pitts, B. J. Reactions at interfaces as a source of sulfate formation in sea-salt particles. *Science* **2003**, *301* (5631), 340–344.

(21) Wilson, T. R. S., Salinity and the major elements of seawater, in *Chemical Oceanography*, 2nd ed., edited by J. P. Riley G. Skirrow, Academic Press, New York, Vol. 1, pp 365−413, 1975.

(22) Hopkins, R. J.; Desyaterik, Y.; Tivanski, A. V.; Zaveri, R. A.; Berkowitz, C. M.; Tyliszczak, T.; Gilles, M. K.; Laskin A. Chemical speciation of sulfur in marine cloud droplets and particles: Analysis of individual particles from the marine boundary layer over the California current. *J. Geophys. Res.* **2008**, *113*, D04209, doi:10.1029/2007JD008954.

(23) Geng, H.; Jung, H.-J.; Park, Y. M.; Hwang, H. J.; Kim, H. K.; Kim, Y. J.; Sunwoo, Y.; Ro, C.-U. Morphological and chemical composition characteristics of summertime atmospheric particles collected at Tokchok Island, Korea. *Atmos. Environ.* **2009**, *43* (21), 3364–3373.

(24) Kukui, A.; Borissenko, D.; Laverdet, G.; Le Bras, G. Gas-phase reactions of OH radicals with dimethyl sulfoxide and methane sulfinic acid using turbulent flow reactor and chemical ionization mass spectrometry. *J. Phys. Chem. A* **2003**, *107* (30), 5732–5742.

(25) Gaston, C. J.; Pratt, K. A.; Qin, X.; Prather, K. A. Real-time detection and mixing state of methanesulfonate in single particles at an inland urban location during a phytoplankton bloom. *Environ. Sci. Technol.* **2010**, *44* (5), 1566–1572.

(26) Shon, Z.-H.; Davis, D.; Chen, G.; Grodzinsky, G.; Bandy, A.; Thornton, D.; Sandholm, S.; Bradshaw, J.; Stickel, R.; Chameides, W.; Kok, G.; Russell, L.; Mauldin, L.; Tanner, D.; Eisele, F. Evaluation of the DMS flux and its conversion to SO_2 over the Southern Ocean. *Atmos. Environ.* **2001**, *35*, 159–172.

(27) Boyd, P. W.; Watson, A. J.; Law, C. S.; Abraham, E. R.; Trull, T.; Murdoch, R.; Bakker, D. C.; Bowie, A. R.; Buesseler, K. O.; Chang, H.; Charette, M.; Croot, P.; Downing, K.; Frew, R.; Gall, M.; Hadfield, M.; Hall, J.; Harvey, M.; Jameson, G.; LaRoche, J.; Liddicoat, M.; Ling, R.; Maldonado, M. T.; McKay, R. M.; Nodder, S.; Pickmere, S.; Pridmore, R.; Rintoul, S.; Safi, K.; Sutton, P.; Strzepek, R.; Tanneberger, K.; Turner, S.; Waite, A.; Zeldis, J. A mesoscale phytoplankton bloom in the polar Southern Ocean stimulated by iron fertilization. *Nature* **2000**, *407* (6805), 695–702.

(28) Zhuang, G.; Yi, Z.; Duce, R. A. Link between iron and sulfur suggested by the detection of Fe(II) in remote marine aerosols. *Nature* **1992**, *355*, 537–539.

(29) Gervais, F.; Riebesell, U.; Gorbunov, M. Y. Changes in primary productivity and chlorophyll a in response to iron fertilization in the Southern Polar Frontal Zone. *Limnol. Oceanogr.* **2002**, *47* (5), 1324–1335.

(30) Wagenbach, D.; Ducroz, F.; Mulvaney, R.; Keck, L.; Minikin, A.; Legrand, M.; Hall, J. S.; Wolff, E. W. Sea-salt aerosol in coastal Antarctic regions. *J. Geophys. Res.* **1998**, *103* (D9), 10961–10974.

(31) Minikin, A.; Legrand, M.; Hall, J.; Wagenbach, D.; Kleefeld, C.; Wolff, E.; Pasteur, E. C.; Ducroz, F. Sulfur-containing species (sulfate and methanesulfonate) in coastal Antarctic aerosol and precipitation. *J. Geophys. Res.* **1998**, *103* (D9), 10975–10990.

(32) Preunkert, S.; Jourdain, B.; Legrand, M.; Udisti, R.; Becagli, S.; Cerri, O. Seasonality of sulfur species (dimethyl sulfide, sulfate, and methanesulfonate) in Antarctica: Inland versus coastal regions. *J. Geophys. Res.* **2008**, *113* (D15), D15302.